

# Coordination of Brain-Wide Activity Dynamics by Dopaminergic Neurons

Heather K Decot<sup>1,2,10</sup>, Vijay MK Namboodiri<sup>2,3,10</sup>, Wei Gao<sup>4,5</sup>, Jenna A McHenry<sup>2</sup>, Joshua H Jennings<sup>1,2</sup>, Sung-Ho Lee<sup>5,6</sup>, Pranish A Kantak<sup>2</sup>, Yu-Chieh Jill Kao<sup>5,6</sup>, Manasmita Das<sup>5,6</sup>, Ilana B Witten<sup>7</sup>, Karl Deisseroth<sup>8</sup>, Yen-Yu Ian Shih<sup>\*,1,5,6,9</sup> and Garret D Stuber<sup>\*,1,2,3</sup>

<sup>1</sup>Curriculum in Neuroscience, University of North Carolina at Chapel Hill, Chapel Hill, NC, USA; <sup>2</sup>Departments of Psychiatry and Cell Biology and Physiology, Chapel Hill, NC, USA; <sup>3</sup>Neuroscience Center, University of North Carolina at Chapel Hill, Chapel Hill, NC, USA; <sup>4</sup>Department of Radiology, University of North Carolina at Chapel Hill, Chapel Hill, NC, USA; <sup>5</sup>Biomedical Research Imaging Center, University of North Carolina at Chapel Hill, Chapel Hill, NC, USA; <sup>6</sup>Department of Neurology, University of North Carolina at Chapel Hill, Chapel Hill, NC, USA; <sup>7</sup>Princeton Neuroscience Institute and Department of Psychology, Princeton University, Princeton, NJ, USA; <sup>8</sup>Department of Bioengineering, Stanford University, Stanford, CA; <sup>9</sup>Department of Biomedical Engineering, University of North Carolina at Chapel Hill, Chapel Hill, NC, USA

Several neuropsychiatric conditions, such as addiction and schizophrenia, may arise in part from dysregulated activity of ventral tegmental area dopaminergic (TH<sup>VTA</sup>) neurons, as well as from more global maladaptation in neurocircuit function. However, whether TH<sup>VTA</sup> activity affects large-scale brain-wide function remains unknown. Here we selectively activated TH<sup>VTA</sup> neurons in transgenic rats and measured resulting changes in whole-brain activity using stimulus-evoked functional magnetic resonance imaging. Applying a standard generalized linear model analysis approach, our results indicate that selective optogenetic stimulation of TH<sup>VTA</sup> neurons enhanced cerebral blood volume signals in striatal target regions in a dopamine receptor-dependent manner. However, brain-wide voxel-based principal component analysis of the same data set revealed that dopaminergic modulation activates several additional anatomically distinct regions throughout the brain, not typically associated with dopamine release events. Furthermore, explicit pairing of TH<sup>VTA</sup> neuronal activation with a forepaw stimulus of a particular frequency expanded the sensory representation of that stimulus, not exclusively within the somatosensory cortices, but brain-wide. These data suggest that modulation of TH<sup>VTA</sup> neurons can impact brain dynamics across many distributed anatomically distinct regions, even those that receive little to no direct TH<sup>VTA</sup> input.

*Neuropsychopharmacology* (2017) **42**, 615–627; doi:10.1038/npp.2016.151; published online 14 September 2016

## INTRODUCTION

Midbrain dopaminergic neurons have been reported to encode reward prediction errors (Cohen *et al*, 2012; Schultz, 1998; Steinberg *et al*, 2013) and signal the incentive salience (Berridge and Robinson, 1998) of sensory cues. During reward-seeking behavior, burst firing of these neurons results in phasic dopamine release (Day *et al*, 2007; Phillips *et al*, 2003; Stuber *et al*, 2008) in cortical and limbic terminal fields such as the medial prefrontal cortex and nucleus accumbens (NAc), which in conjunction with other neurotransmitters act to modulate postsynaptic neuronal firing (Gee *et al*, 2012;

Surmeier *et al*, 2007) and promote changes in motivated behavioral output (Salamone *et al*, 2007; Stuber *et al*, 2011; Tsai *et al*, 2009; Tye *et al*, 2013). The direct consequences of dopamine signaling are largely restricted to brain regions that contain appreciable presynaptic fibers that release dopamine, as well as postsynaptic dopamine receptors. However, dopaminergic signaling may also indirectly influence the activity in multiple brain regions, some of which may receive little to no direct dopamine input. By sculpting activity dynamics of neurons that are polysynaptically downstream, ventral tegmental area (VTA) DAergic neurons may thus modulate a much larger functional brain circuit.

In addition to dopamine signaling by natural rewards (Cohen *et al*, 2012; Day *et al*, 2007; Roitman *et al*, 2004, 2008; Schultz, 1998), drugs of abuse increase extracellular dopamine in mesolimbic terminal fields such as the NAc (Di Chiara and Imperato, 1988; Phillips *et al*, 2003; Stuber *et al*, 2005a, 2005b), supporting the notion that aberrant dopamine signaling may have a principal role in mediating the neurobiological and behavioral maladaptations associated with addiction (Pascoli *et al*, 2015). A hallmark feature of addiction is the enhanced salience that sensory stimuli

\*Correspondence: Professor Y-Yi Shih, Departments of Neurology and Biomedical Engineering, Biomedical Research Imaging Center, University of North Carolina at Chapel Hill, Chapel Hill, NC 27599, USA, Tel: +1 919 843 4729, Fax: +1 919 843 4456, E-mail: shihy@unc.edu or Professor GD Stuber, Departments of Psychiatry and Cell Biology and Physiology, Neuroscience Center, University of North Carolina at Chapel Hill, Chapel Hill, NC 27599, USA, Tel: +1 919 843 7140, Fax: +1 919 966 1050, E-mail: gstuber@med.unc.edu

<sup>10</sup>These authors contributed equally to this work.

Received 10 May 2016; revised 15 July 2016; accepted 26 July 2016; accepted article preview online 12 August 2016

acquire when paired with drugs of abuse, which can promote drug craving (Childress *et al*, 1999; Kalivas and Volkow, 2005; Koob and Volkow, 2009; Volkow *et al*, 2004). This enhanced salience triggered by drug-associative cues likely involves phasic dopamine release as drug-associated cues can directly evoke robust dopamine release events in the NAC that are modulated by the cue–drug association (Phillips *et al*, 2003b; Stuber *et al*, 2005b). Although release of dopamine during this process would be predicted to have direct effects on striatal neuronal activity, it is also possible that dopamine release, when paired with a sensory stimulus, may modulate the salience or value of that particular stimuli via effects that occur in brain regions downstream of circuits that are directly modulated by dopamine. Indeed, a previous report demonstrated that electrical stimulation of the VTA, time-locked to an auditory stimulus presentation, resulted in enlarged sensory representation of that particular stimulus within the auditory cortex (Bao *et al*, 2001). Thus, previous work implies that dopamine signaling may modulate cue-evoked behavioral responding by acting both at the site of release in striatal targets and by changing brain activity in potentially many other brain nuclei that do not directly receive appreciable dopamine input.

To further investigate these two complementary ideas, we studied how *in vivo* modulation of VTA dopaminergic neurons altered brain-wide activity patterns using *in vivo* optogenetics coupled with functional magnetic resonance imaging (fMRI) (Domingos *et al*, 2011; Ferenczi *et al*, 2016; Gerits *et al*, 2012; Kahn *et al*, 2011; Lee *et al*, 2010). We first tested whether selective optogenetic stimulation of VTA dopaminergic (TH<sup>VTA</sup>) neurons produced changes in fMRI signals and altered activity within multiple, anatomically distinct regions that directly receive dopamine input. This approach capitalizes on the genetic specificity offered by optogenetic strategies and the capability of resolving brain-wide macroscale patterns of activity afforded by fMRI. Using a standard generalized linear model (GLM) analysis approach, our results indicate that selective activation of TH<sup>VTA</sup> neurons produces dopamine receptor-dependent increases in CBV signals in well-established dopaminergic terminal fields such as the striatum. In contrast, whole brain voxel-based principal component analysis (PCA) of the same data set, which allowed us to survey changes in brain-wide activity, revealed that dopaminergic modulation activates many additional anatomically defined regions throughout the brain. Using our developed PCA-fMRI approach, we also explored how dopamine stimulation coupled with a discrete sensory stimulus affects the representation of that stimulus throughout the entire brain. We reveal that explicit pairing of TH<sup>VTA</sup> neuron activity with forepaw stimulation markedly alters the brain-wide sensory representation of that stimulus. These findings provide new insight into the global adaptation in neurocircuit function associated with the attribution of salience to sensory cues in the environment.

## MATERIALS AND METHODS

### Experimental Subjects and Stereotactic Surgery

All procedures were conducted in accordance with the Guide for the Care and Use of Laboratory Animals, as adopted by

the National Institutes of Health, and with approval of the Institutional Animal Care and Use Committee at the University of North Carolina (UNC). Adult (400–450 g) male *tyrosine hydroxylase* (TH)-ires-cre Long–Evans rats were group housed until surgery and were maintained on a 12-h light cycle (lights off at 1900 hours) with mild food restriction to maintain ~90% body weight during the duration of the study. To target dopamine neurons within the midbrain, TH-ires-cre rats were endotracheally intubated and ventilated using a small animal ventilator (SAR-830/PA; CWE, Moore, PA) with ~1.5% isoflurane in medical air before being placed into a stereotactic frame (Model 962; Kopf Instruments, Tujunga, CA). For all experiments, rats were microinjected with quadruple injections of 1  $\mu$ l of purified and concentrated adeno-associated virus (~10<sup>12</sup> infectious units per ml, packaged by the UNC Vector Core Facility) into the VTA using the following coordinates (in mm from bregma): –5.4 and –6.2 anterior/posterior,  $\pm$ 0.7 medial/lateral, and –8.4 and –7.4 dorsal/ventral. VTA dopaminergic neurons were transduced with an AAV5 carrying a Cre-inducible expression cassette encoding channelrhodopsin-2 (ChR2) fused to an enhanced yellow fluorescent protein (eYFP) under the control of the EF1 $\alpha$  promoter (AAV5-DIO-ChR2-eYFP; TH<sup>VTA</sup>::ChR2 rats) or only eYFP (AAV5-DIO-eYFP; TH<sup>VTA</sup>::control rats). 200  $\mu$ m multimode chronic optical fibers were stereotactically implanted bilaterally at a 10° angle directly above the VTA using the following stereotactic coordinates: –5.8 mm to bregma,  $\pm$ 2.14 mm lateral to midline, and –7.8 mm ventral to the skull surface. The time from virus injection to the start of the MRI experiments was 5–6 weeks for all subjects.

### fMRI Procedures

MRI was performed using a 9.4 T Bruker BioSpec system with a BGA-9S gradient insert (Bruker Corp., Billerica, MA) at the UNC Biomedical Research Imaging Center (BRIC). On the day of MRI experiments, each rat was endotracheally intubated and ventilated with ~1.5% isoflurane in medical air. The ventilation rate and volume were adjusted via a capnometer (Surgivet v9004; Smith Medical, Waukesha, WI) to maintain end-tidal CO<sub>2</sub> (EtCO<sub>2</sub>) within a range of 3.0  $\pm$  0.2%. Noninvasive EtCO<sub>2</sub> values were previously calibrated against invasive blood-gas samplings under identical baseline conditions, resulting in an arterial pCO<sub>2</sub> of 37.6  $\pm$  4.7 mm Hg (Shih *et al*, 2013). Heart rate and oxygen saturation (SpO<sub>2</sub>) were continuously monitored by a non-invasive MouseOx Plus System with MR-compatible sensors (STARR Life Science Corp., Oakmont PA) and maintained within normal ranges (~280 b.p.m. and >96%, respectively). Rectal temperature was maintained at 37  $\pm$  0.5 °C with a warm-water circulating pad. Black tape was placed over the eyes and a masking light was directed into the face of each rat to minimize visual stimulation during laser light delivery.

A home-made surface coil with an internal diameter of 1.6 cm placed directly over the head was used as an RF transceiver. Magnetic field homogeneity was optimized using standard FASTMAP shimming with first-order shims on an isotropic voxel of 7  $\times$  7  $\times$  7 mm<sup>3</sup> encompassing the imaging slices. A RARE T<sub>2</sub>-weighted image was taken in the mid-sagittal plane to localize the anatomical position by identifying the anterior commissure at 0.36 mm posterior

to bregma. To ensure anatomical consistency of the imaging data, 12 coronal slices were acquired using  $T_2$ -weighted imaging, with the fourth slice from the anterior direction aligned with the anterior commissure. A RARE sequence (spectral width = 47 kHz, TR/TE = 2500/33 ms, FOV =  $2.56 \times 2.56$  cm<sup>2</sup>, slice thickness = 1 mm, matrix =  $256 \times 256$ , RARE factor = 8, and number of averages = 8) was used to confirm optical fiber position with reference to the cortical surface, midline, and the anterior commissure. For functional scans, single shot gradient echo-EPI sequence (spectral width = 300 kHz, TR/TE = 1000/8.1 ms, FOV =  $2.56 \times 2.56$  cm<sup>2</sup>, slice thickness = 1 mm, matrix =  $80 \times 80$ , providing temporal resolution = 1 s) was used.

During fMRI, dexmedetomidine (0.1 mg/kg per h) and pancuronium bromide (1.0 mg/kg per h) were infused intraperitoneally and isoflurane was lowered to 0.5% 30 min after the infusion began (Fukuda *et al*, 2013). Cerebral blood volume (CBV)-weighted fMRI (Mandeville *et al*, 1998) was achieved by injecting Feraheme (AMAG Pharmaceuticals, Lexington, MA) at a dose of 30 mg Fe/kg via a tail vein catheter. CBV-weighted fMRI was chosen over the more conventional blood oxygenation-level-dependent (BOLD) fMRI owing to its ability to provide significantly greater functional sensitivity (Kim *et al*, 2013). Optical fibers were coupled via 3-m patch cables to solid-state lasers (473 nm wavelength) located outside the MRI room delivering ~ 10 mW light to each hemisphere of the VTA. Evoked fMRI scans were acquired for 100 s during which photostimulation was applied in a 20-s OFF, 10-s ON, 30-s OFF, 10-s ON, and 30-s OFF pattern. Subjects underwent two to five repeated trials at each photostimulation frequency (10, 20, 30, and 40 Hz at 5 ms pulse width) in a pseudorandom manner. Dopamine D1 receptor antagonist, SCH23390 (0.6 mg/kg) (Sigma), was injected intravenously to explore its effects on stimulus-evoked CBV changes observed in TH<sup>VTA</sup>::ChR2 rats. This SCH23390 dose was chosen because it was comparable to the dose used in a similar fMRI study (Marota *et al*, 2000). For paired forepaw and optogenetic stimulation experiments, electrical forepaw stimulation was applied using two needle electrodes inserted under the skin of the right forepaw of each subject. The stimulation was applied in a 20-s OFF, 10-s ON, and 70-s OFF pattern. To measure the frequency dependence of the stimulus-evoked activation, subjects underwent two to five repeated trials at the following frequencies: 1, 3, 9, 15, and 21 Hz with a fixed pulse width of 0.3 ms and a current of 1.5–3.0 mA (prepairing). Then, a repeated pairing of forepaw electrical stimulation at 9 Hz with 30 Hz optogenetic stimulation of VTA dopamine neurons was performed with an initial 20-s OFF, followed by 20 blocks of 10-s ON and 70-s OFF. Finally, changes in CBV signals and frequency dependence in response to all forepaw stimuli frequencies were reassessed (postpairing).

## Data Processing and Statistical Analysis

*GLM-based stimulation analysis.* fMRI data analyzed using a GLM were processed using Matlab (Math-Works, Natick, MA) and Statistical Parametric Mapping codes, with the pipeline similar to our previous publications (Lai *et al*, 2015; Shih *et al*, 2014a, b; Younce *et al*, 2014). Automatic coregistrations were applied to realign time-series data within subjects to correct subtle drift of EPI images and

then again across subjects to provide group-based fMRI maps. Data were analyzed using the Analysis of Functional Neuroimages (AFNIs) with the framework of GLM (Cox, 1996; Worsley and Friston, 1995; Worsley *et al*, 2002), with false discovery rate correction to adjust for the multiple comparisons of fMRI maps ( $p < 0.05$ ). The stimulation paradigm was convoluted with response model of Feraheme (Leite *et al*, 2002) injection in AFNI package to get an ideal model of hemodynamic response (Supplementary Figure S2F). Regions of interest (ROIs) were placed on the dorsal striatum bilaterally to extract fMRI time-course data after the images were coregistered. For pairing experiments, ROI was placed on the contralateral somatosensory cortex (S1). To control for Feraheme metabolism over the course of each experiment, the following equations were used to calculate  $\Delta$ CBV: Baseline  $\Delta R_2^* = -1/TE \ln(S_{\text{prestim}}/S_0)$ , where  $S_{\text{prestim}}$  and  $S_0$  represents MR signal intensity after and before Feraheme injection. Stimulus evoked  $\Delta R_2^* = -1/TE \ln(S_{\text{stim}}/S_{\text{prestim}})$ , where  $S_{\text{stim}}$  and  $S_{\text{prestim}}$  are the MR signal intensities during and before stimulation, respectively. CBV changes were calculated by dividing stimulus-evoked  $\Delta R_2^*$  by baseline  $\Delta R_2^*$  values. The effect of optogenetic and forepaw stimulation frequency on  $\Delta$ CBV change was calculated by averaging CBV values from the first 20 s time points during each stimulation epoch. Two-way ANOVA tests followed by Bonferroni *post hoc* comparisons were applied for comparisons with more than two groups. All data were expressed as mean  $\pm$  SEM and significance was set at  $p < 0.05$ .

*PCA-based stimulation analysis.* PCA analysis pipeline for data analyzed using this method within this manuscript was written in python 2.7 using numpy and scikitlearn packages. All analysis code is available in well-documented iPython notebooks (see Supplementary Information).

*Histology, immunohistochemistry, and microscopy.* Rats were deeply anesthetized with pentobarbital, and transcardially perfused with phosphate-buffered saline (PBS) followed by 4% (weight/volume) paraformaldehyde in PBS. Brains were postfixed in 4% paraformaldehyde for 24 h and transferred to 30% sucrose in ddH<sub>2</sub>O for 48 h. Forty micrometers of brain sections were collected and blocked in 10% normal donkey serum in 0.1% Triton (200:1800  $\mu$ l) for 1 h. Sections were then incubated in primary antibody (TH, 1:500 Pel Freeze; made in sheep) for 48 h at 4 °C. Following 4  $\times$  10 min PBS washes, the sections were incubated in secondary antibody (Dylight 649 donkey anti-sheep, 1:800; Jackson ImmunoResearch Laboratories, West Grove, PA) for 24 h at 4 °C. All sections were coverslipped with Fluoroshield with DAPI (Sigma Aldrich, St Louis, MO). Z-stack and tiled images of mounted brain sections were visualized using Zeiss LSM 710 confocal microscope with a  $\times 20$  or  $\times 63$  objective.

## RESULTS

### Viral Targeting of VTA Dopaminergic Neurons in TH-Cre Rats

To selectively stimulate TH<sup>VTA</sup> neurons *in vivo*, we introduced the light-gated cation channel, ChR2 conjugated to eYFP (ChR2-eYFP), selectively into VTA neurons in transgenic rats that express Cre recombinase under the

control of the *tyrosine hydroxylase* (TH) gene promoter (Witten *et al*, 2011) using established viral procedures (Jennings *et al*, 2013) (Figure 1a). Because of a recent report of ectopic targeting of VTA neurons in TH-Cre mouse lines (Lammel *et al*, 2015), we performed a detailed quantitative assessment of viral targeting to TH+ neurons in the TH-Cre rat line across the anterior/posterior and medial/lateral subregions of the midbrain (Figures 1a–c). We quantified the location of all neurons within anterior, middle, and posterior sections expressing only eYFP (eYFP+/TH–), TH (eYFP–/TH+), and neurons that expressed both (eYFP+/TH+) ( $n = 9$  sections in  $n = 3$  rats). Collapsed across the anterior–posterior axis containing the VTA, we observed highly specific viral transduction of TH+ neurons ( $97.4 \pm 1.0\%$ ,  $n = 9$  slices from  $n = 3$  rats; Figure 1d). Notably, few neurons that were eYFP+, but showed TH immunoreactivity that could not be resolved above background, tended to reside in the anterior VTA or ventral to the VTA in the interpeduncular nucleus (Figure 1c). Based on stereotactic optical fiber placement directly above the VTA and predicted transmission of light power at 473 nm through the brain tissue, it was unlikely that light from the optical fiber tip would spread to illuminate and activate those few neurons in the IPN that were eYFP+/TH– (Aravanis *et al*, 2007). In TH-Cre rats injected with AAV-DIO-ChR2-eYFP, we also observed substantial innervation of striatal subregions including the dorsal medial striatum (DMS) and the NAc (Figures 1e and f). These results further validate the use of TH-Cre rats for targeted manipulation of TH<sup>VTA</sup> neurons, with minimal targeting to TH– neurons in and around the VTA.

### Whole Brain Analysis Following TH<sup>VTA</sup> Neuron Stimulation

In separate rats, we expressed ChR2-eYFP or eYFP alone in TH<sup>VTA</sup> neurons and implanted bilateral optical fibers directly above the VTA for light delivery (Sparta *et al*, 2012) (Supplementary Figure S1). Following recovery from surgery and sufficient time for adequate ChR2-eYFP expression in TH<sup>VTA</sup> neurons, sedated rats were interfaced with a custom-built surface coil, placed in a 9.4 Tesla small animal MRI scanner, and the implanted optical fibers were connected to 473 nm diode-pumped solid-state lasers located outside the MRI room (Figure 2a). Following acquisition of 12, coronal T<sub>2</sub>-weighted anatomical image sections from each animal (Supplementary Figure S1B), CBV-weighted fMRI (Kim *et al*, 2013; Mandeville *et al*, 1998; Shih *et al*, 2009; Smirnakis *et al*, 2007) data, which indirectly measures neuronal activity by detecting changes in hemodynamic signals accompanying vascular responses, were acquired using a single-shot echo planar imaging sequence at 1 s temporal resolution. To produce sustained, dopaminergic signaling, TH<sup>VTA</sup> neurons were optically stimulated at 10–40 Hz for 10 s (Supplementary Figures S2A and C). With these parameters we measured CBV responses across 12 continuous coronal slices of 1 mm thickness, each encompassing nearly the entire cerebrum. Using a standard GLM to compare each voxel's activity trace to a predefined stimulation template or hemodynamic response function (Ferenczi *et al*, 2016; Leite *et al*, 2002; Monti, 2011) (Supplementary Figure S2E), optogenetic stimulation of TH<sup>VTA</sup> neurons

produced pronounced CBV increases in striatal brain regions in a frequency-dependent manner relative to control animals that received laser-light delivery, but only expressed eYFP in TH<sup>VTA</sup> neurons (Supplementary Figure S2). Further, systemic administration of a dopamine D1 receptor (D1R) antagonist, SCH23390, significantly attenuated CBV signals caused by TH<sup>VTA</sup> optogenetic stimulation (Supplementary Figure S2B). The D1R antagonist had no significant effect on eYFP control animals, verifying that the antagonist is specifically blocking the TH<sup>VTA</sup> neuron-stimulated signal, and not causing a stimulation-independent effect on the baseline (Supplementary Figure S2C). Taken together, these data show that selective activation of TH<sup>VTA</sup> neurons produces dopamine receptor-dependent signaling that result in increased CBV signals in dopaminergic terminal fields.

Owing to the lack of a well-defined dopamine-evoked hemodynamic response function and to mitigate the biases and assumptions imposed by traditional fMRI whole brain signal analysis, we developed an analytical pipeline by which all imaging voxels (35 182 per brain) and associated CBV-weighted time-series data were subjected to PCA factorization (Andersen *et al*, 1999; Freeman *et al*, 2014) (Figure 2c and see Supplementary Information). This resulted in a substantial reduction of the dimensionality of the spatio-temporal data set from 35 182 down to 75 PCs that explained 80% of the variance of the data. Importantly, the first PC alone explained 7% of the variance of data collected from ChR2-eYFP rats. The percent variance of the data explained by each subsequent PC reached an asymptote by 3–4 PCs (Figure 2d).

The first PC plotted as a function of time represented the effect of TH<sup>VTA</sup> optogenetic stimulation as it significantly increased from the baseline period (0–20 s) in each poststimulation period (30–60 and 70–100 s) ( $t(48.0) = 11.69$ ,  $p < 0.001$ , Welch's *t*-test for poststimulation period 1 and  $t(38.7) = 7.15$ ,  $p < 0.001$ , Welch's *t*-test for poststimulation period 2; Figure 2e), largely recapitulating the ROI analysis of striatal signals shown in Supplementary Figure S2A. In contrast, data collected from rats only expressing eYFP in TH<sup>VTA</sup> neurons showed no significant poststimulation response. As the weight of a voxel to a given PC reflects the correlation between the voxel's and the PC time-series signals (Yamamoto *et al*, 2014), we hypothesized that a given voxel's contribution to PC1 would highly correlate with the raw signal intensity for that voxel in the poststimulation period exclusively in data collected from ChR2-eYFP rats. Supporting this, a highly significant positive Pearson's correlation between these two variables was observed in the ChR2-eYFP group ( $R^2 = 0.68$ , slope = 1.12,  $p < 0.001$ ). In contrast, the eYFP group showed a slight, but significant negative correlation ( $R^2 = 0.08$ , slope = –0.28,  $p < 0.001$ ; Figure 2f). We then ranked all voxels as a function of PC1 weight and plotted the time series for the top 500 voxels for both ChR2-eYFP and eYFP groups (Figure 2g). Comparing these results to the top 500 voxels ranked by their mean poststimulation response shows a marked enhancement of the temporal structure of the data (Supplementary Figure S3B), further supporting our PCA-based analysis approach.

We then mapped the voxels that significantly contributed to the PC representing the stimulation effect back to a T<sub>2</sub>-weighted reference brain atlas (Figure 2h). This also showed

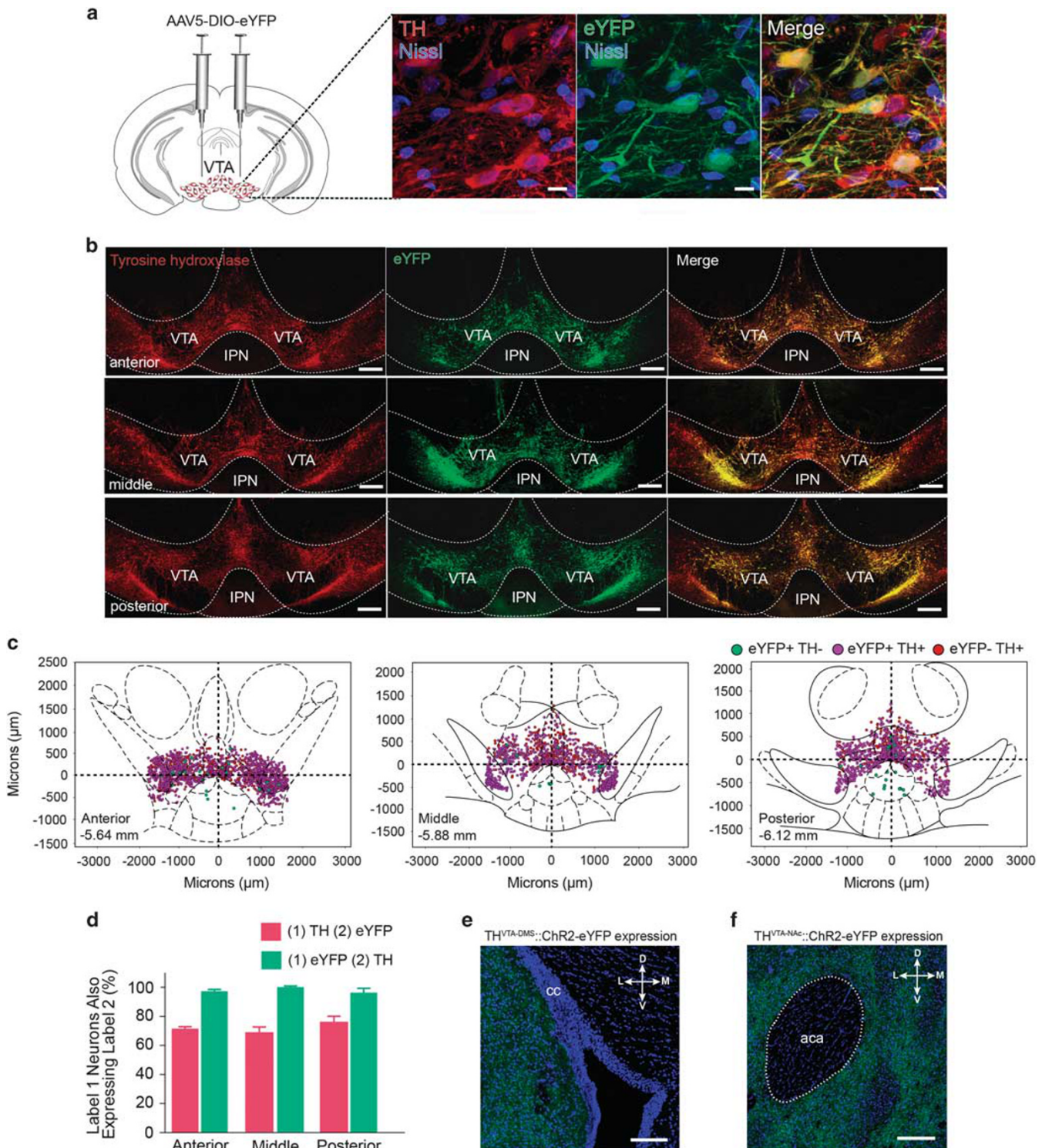


**Figure 1** Viral targeting of ventral tegmental area (VTA) dopaminergic neurons in tyrosine hydroxylase-cre (TH-cre) rats. Confocal images (objectives (a)  $\times 63$  and (b)  $\times 20$ ) depicting enhanced yellow fluorescent protein (eYFP) expression (green) following injection of a Cre-inducible virus into the VTA in TH-cre rats. Merged images reveal colocalization of eYFP and TH; red = TH; blue = Nissl stain. (c and d) Quantification of the location of all neurons within anterior, middle, and posterior slices of the VTA expressing only eYFP (eYFP+/TH-), TH (eYFP-/TH+), and neurons that expressed both (eYFP+/TH+) ( $n=9$  sections in  $n=3$  rats). Collapsed across the anterior–posterior axis,  $71.9 \pm 2.1\%$  of TH+ neurons within the VTA also expressed eYFP and  $97.4 \pm 1.0\%$  of eYFP-positive cells also expressed TH. Error bars represent SEM. (e and f) Confocal images showing expression of channelrhodopsin-2-eYFP (ChR2-eYFP) fibers in downstream target regions of the VTA including the dorsomedial striatum (DMS) and nucleus accumbens (NAC) of a TH<sup>VTA</sup>::ChR2 rat. Scale bars, 200 and 500  $\mu\text{m}$ , respectively. Aca, anterior commissure; cc, corpus callosum; IPN, interpeduncular nucleus.

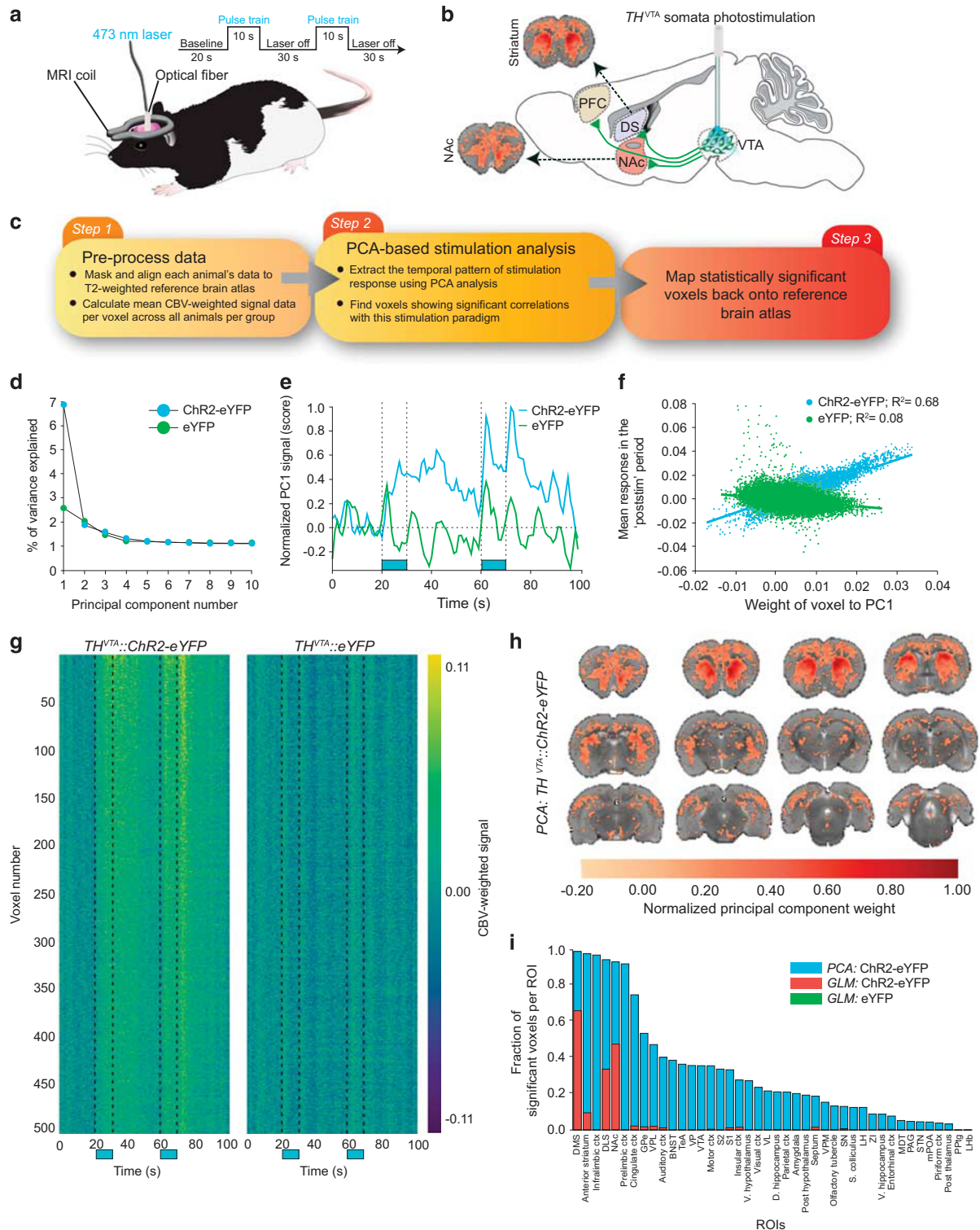


**Figure 2** Whole brain analysis of the effect of ventral tegmental area dopaminergic ( $TH^{VTA}$ ) neuron stimulation. (a and b) Diagram of the experimental setup. (c) Schematic of the analysis pipeline (see Supplementary Information). (d) The percentage of variance captured by each principal component (PC) showing that the difference in variance explained between consecutive PCs is minimal after 2–3 PCs. (e) The normalized trace (score) of the first PC for both experimental and control groups showing clear poststimulation response only for the experimental group. The normalization was carried out such that the maximum score across both PCs is 1 (at 72 s for the experimental group). (f) A scatter plot showing the correlation between the weight of a voxel to the first PC and its mean poststimulation response for both groups. (g) The raw voxel traces for the top 500 voxels contributing to the first PC for both groups. (h) The map showing the significant voxels contributing to the first PC vector for the experimental group, for which a significant poststimulation response was identified (see Supplementary Information). There was no PC for the control group that represented any significant poststimulation effect. PC weights were divided by the maximum PC weight for normalization. (i) Individual regions of interest (ROIs) and their fractional contribution (see Supplementary Information) to the PC representing the stimulation effect is shown in cyan. Red and green show the fraction of significant voxels that shows significant generalized linear model (GLM) coefficients for the experimental and control group, respectively.

a marked enhancement of brain-wide activation patterns evoked by the stimulation compared with standard GLM-based significant voxels (Supplementary Figure S3C and D). In order to then place all significant PC1-weighted voxels back to defined brain regions, we annotated all 12 T<sub>2</sub>-weighted brain slices into 42 anatomical subregions based on two widely used rodent brain atlases (Lein *et al*, 2007; Paxinos and Watson, 2005), taking into account the spatial resolution of fMRI (Supplementary Figure S4). Extracted significant voxels (based on PCA and GLM) mapped to numerous diverse brain regions (Figure 2i). All GLM-extracted voxels largely fell into ROIs within striatal subregions and frontal cortices as predicted based on innervation patterns of TH<sup>VTA</sup> neurons (Swanson, 1982) (Figures 1e and f). However, significant PCA-extracted voxels represented a substantially larger fraction of each ROI within these subregions, further highlighting the enhanced sensitivity of this method. Furthermore, many additional brain regions were identified with a high fraction of significant voxels including basal ganglia, basal forebrain, and sensory cortical regions (Figure 2i). Interestingly, intravenous injection of the D1R antagonist not only significantly attenuated CBV signals within striatal target regions but it also prevented stimulation-induced alterations in brain areas that do not directly receive TH<sup>VTA</sup> input (Supplementary Figures S3E and F). To investigate these effects at a more physiologically relevant stimulation period, TH<sup>VTA</sup> neurons were optically stimulated at 30 Hz for 1 s in a subset of animals (Supplementary Figure S5). PCA-based analysis of this data set revealed that selective stimulation of TH<sup>VTA</sup> neurons for 1 s caused activation in fewer pixels across the brain. Interestingly, while the majority of activated pixels were in striatal target regions, some of the regions that showed enhancement at 10 s stimulation also showed slight activation at 1 s. Collectively, this analytical approach reveals for the first time that increased dopaminergic activity produces dispersed effects not only in brain regions that directly receive TH<sup>VTA</sup> input but also in numerous accessory regions not typically associated with direct VTA DAergic modulation.

### Whole Brain Analysis of Forepaw Stimulation Pre and Post Pairing with TH<sup>VTA</sup> Neuron Stimulation

In pathological conditions, such as addiction and schizophrenia, aberrant dopaminergic activity may act to over-enhance the salience of particular intrinsic and extrinsic stimuli (Berridge and Robinson, 1998; Kapur, 2003). Nonspecific stimulation of the VTA can also alter cortical plasticity (Bao *et al*, 2001; Gee *et al*, 2012; Lewis and O'Donnell, 2000; Otani *et al*, 2003); however, it is unclear whether explicit pairing of TH<sup>VTA</sup> activity with a discrete sensory stimulus alters the brain-wide sensory representation of that stimulus. Thus, in a new cohort of rats we tested whether somatosensory representations measured with fMRI was affected by coincidental and selective TH<sup>VTA</sup> activity (Supplementary Figure S6). We first measured changes in CBV signals in response to a range of forepaw stimulation frequencies. We then paired a single forepaw stimulation frequency (9 Hz) with 30 Hz optogenetic stimulation of TH<sup>VTA</sup> neurons 20 times (one pairing every 70 s). Following the pairing protocol, we reassessed changes in CBV signals in

response to all forepaw stimuli frequencies (Figure 3a). Forepaw stimulation produced time-locked CBV increases in the contralateral somatosensory cortex ROI in a frequency-dependent manner. Following pairing of 9 Hz forepaw stimulation with TH<sup>VTA</sup> activity, there was a selective enhancement in CBV signals in response to 9 Hz subsequent forepaw stimulation compared with other non-paired frequencies and data from control animals that received laser light delivery, but did not express Chr2 in TH<sup>VTA</sup> neurons (Figures 3b–e and Supplementary Figure S7).

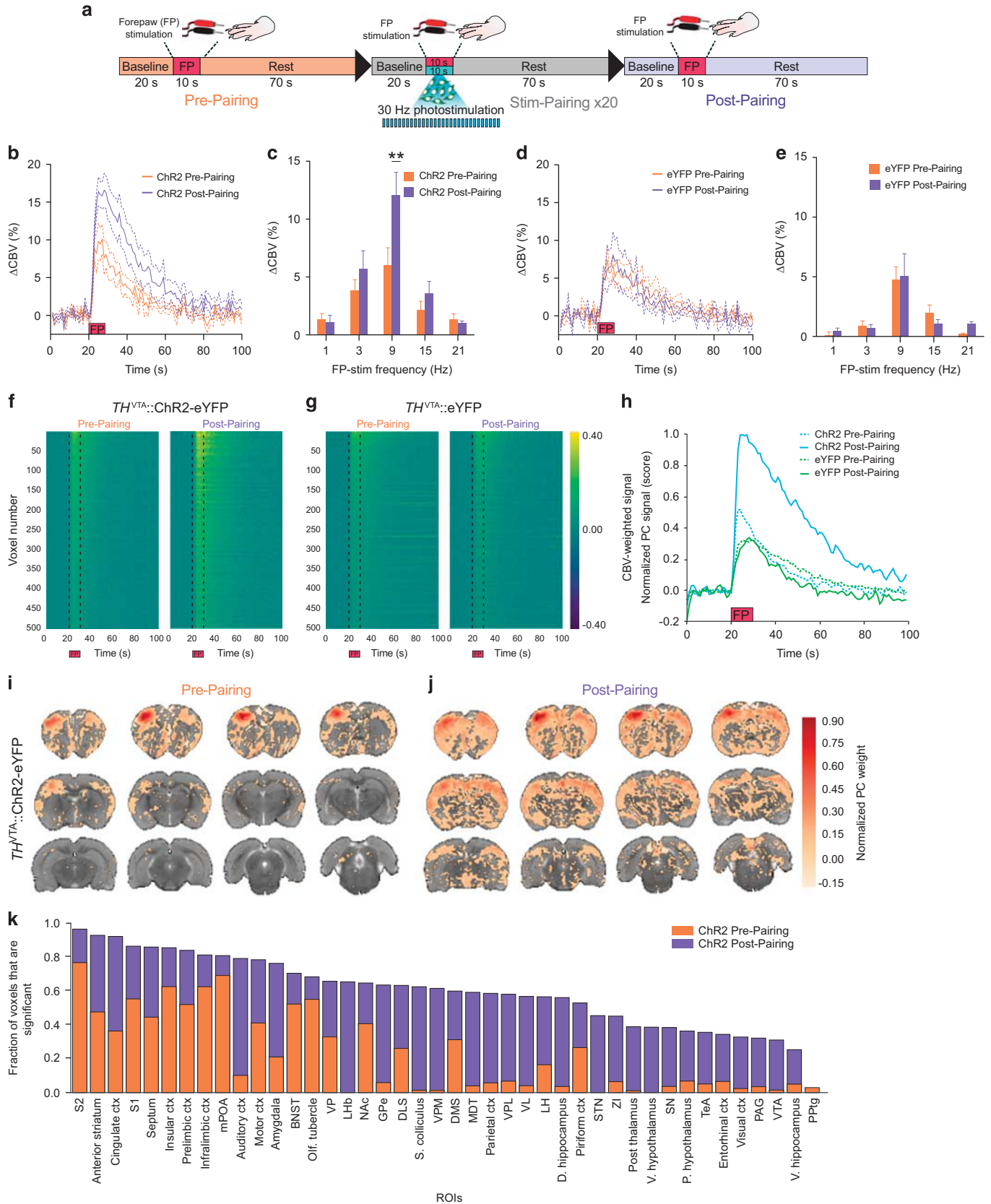
To assess whole brain activity patterns before and after forepaw-TH<sup>VTA</sup> pairing, we applied the PCA pipeline described above (Figure 2c) to this data set. PC1 signal intensity evoked by forepaw stimulation was significantly enhanced following pairing in the Chr2-eYFP group ( $t(18)=19.484$ ,  $p<0.001$ ) but not to eYFP controls ( $t(18)=0.660$ ,  $P=0.52$  two-tailed  $t$ -test of the mean response in the stimulation period; Figures 3f–h and Supplementary Figure S8). Significant voxel weights to the PC1 vector remapped back to the reference atlas revealed a striking enhancement of the fMRI measured sensory representation of forepaw stimulation induced by the pairing protocol (Figures 3i–k). To determine whether repeated TH<sup>VTA</sup> forepaw stimulation pairing gradually enhanced the representation as a function of each pairing, we also calculated the PC fMRI signal for each TH<sup>VTA</sup>-forepaw pairing (20 total). Normalized to the maximum PC signal evoked by forepaw stimulation signals after the pairing, we observed that the first and all subsequent TH<sup>VTA</sup> forepaw stimulation pairings produced an increase in the PC signal in Chr2-eYFP rats relative to eYFP controls (Figure 4a). This is further shown by plotting the ratio of each evoked response per pairing between Chr2-eYFP and eYFP groups (Figure 4b). For either group, normalizing the PC signal to the respective prepairing forepaw response revealed a gradual habituation of the signal with increasing number of pairings (Figure 4c). Collectively, these data suggest that forepaw stimulation paired with dopaminergic activity enhances the PC-fMRI signal gain during pairing as well as the subsequent brain-wide representation of sensory stimuli.

### DISCUSSION

It is well known that midbrain dopaminergic neuronal activation produces neuronal excitation and plasticity in striatal target regions. However, it is not yet clear whether the effect of elevated dopaminergic signaling is limited to these areas. This is an important question to address as it might shed light on the extent of anomalous activity seen in disorders such as addiction and schizophrenia. Two reports, using similar opto-fMRI methods, have shown that stimulation of VTA dopamine neurons produce BOLD signal changes locally within the VTA (Domingos *et al*, 2011) and the striatum (Ferenczi *et al*, 2016). Through our development of novel analytic methods, we extend these findings to show that fMRI-related signal changes are not restricted to these regions but occur brain wide. Our findings suggest that large-scale brain-wide activity dynamics, measured across many distinct neuroanatomical regions, are also directly or indirectly regulated by the activity of VTA dopaminergic neurons *in vivo*. In addition, dopaminergic activity, coincidental with a

particular sensory stimulus, enhanced stimulus-specific neuronal representations brain wide. Previous work has largely focused on the timing at which dopaminergic activity occurs

during ongoing behavior (Cohen *et al*, 2012; Day *et al*, 2007; Phillips *et al*, 2003; Schultz, 1998; Stuber *et al*, 2008) as well as cellular mechanisms by which dopamine signaling can alter



the function of individual neurons (Gee *et al*, 2012; Jacob *et al*, 2013; Lewis and O'Donnell, 2000; Marder, 2012). Although we can state that changes in the brain-wide signal are a result of direct stimulation of VTA TH-expressing neurons, we cannot exclude an effect from coincidental signaling by glutamate/GABA that may also be released from VTA dopaminergic neurons (Chuhma *et al*, 2004; Hnasko *et al*, 2010; Lavin *et al*, 2005; Stuber *et al*, 2010; Tritsch *et al*, 2012, 2014). Nevertheless, in the presence of a D1R antagonist, the extent of activation because of TH<sup>VTA</sup> stimulation reduced significantly, with only a few non-striatal voxels showing significant responses (Supplementary Figure S3F). Indeed, one study (Marota *et al*, 2000) found that SCH23390 alone provided nearly complete blockade of cocaine-induced functional responses in rats, implicating a major role for D1 receptor activation during cocaine administration. Thus, while a significant amount of brain-wide responses is D1R dependent, the residual striatal signal may be dependent on either D2R activation or glutamate/GABA signaling. Although our current work shows that VTA dopaminergic neuronal activity has immediate global consequences, and can remodel brain-wide neuronal activity patterns alone or in the presence of a sensory stimulus, future work is needed to assess how each specific neurotransmitter species that is released by VTA dopaminergic neurons contributes to these phenomena.

To detect and characterize brain-wide activity patterns measured with fMRI following TH<sup>VTA</sup> optogenetic stimulation, we developed a PCA-based approach. This allowed us to reduce the dimensionality of the data in the voxel space, isolate the PC temporal trace that represents the stimulation effect, and then map voxels that contribute significant weight to this PC back to anatomical locations in the brain. The identification of brain voxels that significantly contribute to the PC representing the stimulation effect is effectively similar to the standard GLM approach (Monti, 2011) with notable distinctions. First, standard implementations of GLM require *a priori* specification of an expected stimulation effect. This is traditionally calculated using a hemodynamic response function. However, these functions vary widely across brain regions and species, and additionally are oftentimes derived from task-evoked activity, which is difficult to evaluate brain wide. Moreover, if multiple valid stimulation templates need to be compared (especially in the case with multiple ROIs), power of the analysis can be markedly compromised due to corrections for multiple comparisons. In contrast, our model-free approach is entirely data driven and makes no assumptions of regional

fMRI response specificity, thus making it highly applicable for analyzing brain-wide changes in fMRI activity throughout the entire rat brain in response to time-locked stimulation. Another key benefit of our approach is apparent in the case where the stimulation of interest is not of a sensory region but is instead of a region that releases neuromodulators (e.g. VTA). In this case, modeling the expected stimulation effect as a standard sensory stimulation-based template may be inappropriate as these models assume an exponential decay of the signal immediately following stimulation offset (Supplementary Figure S2F). However, extracting the stimulation response template using PCA (Figure 2e) shows that the stimulation has a prolonged effect even after stimulation offset. Thus, in such cases, we advocate a data-driven approach to extract the stimulation response function. One caveat to our method is that a single PC representing the stimulation effect might also contain shared variation that is independent of the stimulation (eg, intrinsic brain oscillations across regions). This is mitigated within our pipeline by averaging raw fMRI voxels across all animals in each group, as the shared temporal variability that remains in the data is likely only due to the stimulation. Furthermore, the voxel-wise analysis used here addresses some of the concerns and limitations inherent to cluster-based approaches more common in fMRI data analysis (Eklund *et al*, 2016). It is also possible that a single PC does not completely isolate the entire stimulation effect on brain-wide activity. This in theory could be improved by additionally performing independent component analysis within the subspace formed by the top PCs. However, in the current data set, no poststimulation effects were observed outside of the first PC. Taken together, our brain-wide fMRI analysis approach was designed to be easily implemented and sensitive enough to detect stimulation-induced changes in activity across the brain, while also imposing as few assumptions as possible.

The marked sensory pattern emergence following TH<sup>VTA</sup>-forepaw pairing showcases the utility of optogenetic-fMRI experimentation (Figure 3), as findings would have likely been unresolvable using methods that are focused on recording activity in one particular anatomical site. Importantly, our approach can easily be applied to examine the brain-wide consequences of the modulation of any particular neurocircuit node. Our data also suggest that by pairing a sensory stimulus with activation of the TH<sup>VTA</sup> neurons produces an immediate enhancement of the sensory representation (even on the first pairing) while not affecting

**Figure 3** Whole brain analysis of forepaw stimulation pre and post pairing with ventral tegmental area dopaminergic (TH<sup>VTA</sup>) neuron stimulation. (a) Experimental timing diagram. (b) Following pairing of VTA dopaminergic activity with 9 Hz forepaw stimulation (FP) stimulation, there was a significant increase in somatosensory cortex cerebral blood volume (CBV) time-course signal (group main effect:  $F_{1,99} = 183.7, P < 0.0001, n = 7$  rats per group). (c) Pairing VTA dopaminergic activity with 9 Hz FP stimulation selectively enhanced somatosensory CBV signals at 9 Hz compared with other tested frequencies (pairing main effect:  $F_{1,50} = 5.58, P = 0.0219, n = 6-7$  rats per group, double asterisks denote significant ( $P < 0.01$ ) *post hoc* tests between before and after pairing at each frequency). (d) Pairing of VTA laser light delivery with 9 Hz FP in rats only expressing enhanced yellow fluorescent protein (eYFP) did significantly change CBV responses in somatosensory cortex, although the postpairing effect was slightly lower than preparing (group main effect:  $F_{1,99} = 3.976, P = 0.0465, n = 5$  rats per group). (e) Pairing VTA laser light delivery with 9 Hz FP stimulation in rats only expressing eYFP did not alter somatosensory CBV frequency tuning signals (pairing main effect:  $F_{1,50} = 0.02, P = 0.8785, n = 5$  rats). (f and g) Raw voxel traces pre- and postpairing for experimental and control groups, respectively. Postpairing FP shows an enhancement of responses only for the experimental group. The voxels are sorted according to their preparing FP response. The same row represents the same voxels across pre- and postpairing for both groups. (h) PC traces (scores) for all conditions. (i and j) The PC vectors capturing the FP response for pre- and postpairing in the experimental group, showing a marked enhancement of voxels that significantly contribute to the PC representing the FP response. (k) Individual ROIs showing fractional contribution to the PCs representing FP response.

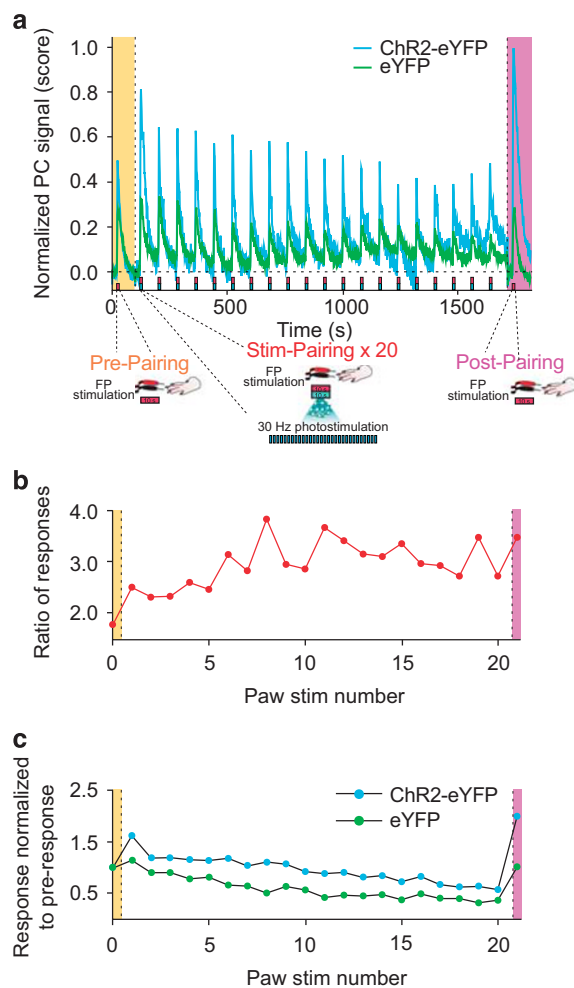


**Figure 4** Evolution of forepaw stimulation pairing response over the course of pairings. (a) The PCs identified (see Supplementary Information) as the ones representing forepaw stimulation response for both groups. The plots show pre- and postpairing forepaw stimulation responses, along with 20 responses during the pairing. (b) The ratio of forepaw stimulation response (difference between the peak response during stimulation and the mean response during a 10 s baseline period before stimulation) for each stimulation between the channelrhodopsin-2-enhanced yellow fluorescent protein (ChR2-eYFP) group and the eYFP group. There is a significant enhancement (positive linear regression) in this ratio as a function of the forepaw stimulation number ( $slope = 0.044$ ,  $P = 0.005$ ,  $R^2 = 0.33$ ). (c) When the forepaw stimulation response for either group is normalized to the prepairing response for the same group, there is significant habituation (negative linear regression) with the number of stimulations during pairing for both groups (ChR2-eYFP:  $slope = -0.041$ ,  $R^2 = 0.895$ ; eYFP:  $slope = -0.034$ ,  $P < 0.001$ ,  $R^2 = 0.831$ ). Importantly, the magnitude of habituation, as measured by the slope of response with respect to pairing number, is statistically indistinguishable for both groups ( $F_{1, 19} = 2.10$ ,  $P = 0.156$ , interaction term in analysis of covariance (ANCOVA)).

the rate of habituation to the sensory stimulus (Figures 4a–c). Our findings provide a foundation and roadmap for future studies that will examine the duration and/or permanence of the brain-wide sensory enhancement by TH<sup>VTA</sup> stimulation as well as examine similar phenomena at the cellular level in a particular brain region using large-scale single-cell calcium imaging approaches.

It is well documented that isoflurane used during opto-fMRI experiments can significantly suppress evoked

hemodynamic responses and do not fully reflect those observed during the awake state (Desai *et al*, 2011; Ferenczi *et al*, 2016). In the present study, animals were continuously infused with a cocktail composed of the  $\alpha_2$ -adrenergic receptor agonist dexmedetomidine and the paralytic agent pancuronium bromide supplemented with very light isoflurane anesthesia (0.5%) over the course of fMRI scan acquisition (Fukuda *et al*, 2013). Although this study attempts to minimize the effects of isoflurane by coupling its use with a sedative and paralytic agent, future studies are needed to replicate our findings in awake animals. We predict that we would see the same enhancement of the sensory representation to an even greater extent if these experiments were performed on awake animals. We also predict that we would still see an enhanced response, albeit to a slightly lesser extent, while using shorter optogenetic stimulation epochs during the TH<sup>VTA</sup>-forepaw pairing, which would better resemble physiologically relevant dopaminergic signaling seen during normal reward processing. Future studies using unpaired stimulations or using another sensory input of another modality following pairing would also be ideal to further investigate whether explicit pairing of dopaminergic signaling and a sensory stimulus is necessary for this effect. It is also important to consider the results of a recent report showing that nonspecific stimulation of the VTA can induce reanimation from general anesthesia, including isoflurane (Solt *et al*, 2014), making it possible that enhanced response to sensory stimuli in the ChR2-eYFP group may be due to reduced depth of anesthesia. Although not recorded, there were no observable changes in autonomic responses (ie, heart rate, EtCO<sub>2</sub>, O<sub>2</sub> saturation) that would indicate animals were becoming more conscious during photostimulation of TH<sup>VTA</sup> neurons.

A hallmark feature of both adaptive learning and addiction is the enhanced salience that sensory stimuli acquire when paired with natural rewards or drugs of abuse. Consistent with this, direct activation of VTA dopaminergic neurons promotes stimulus-driven learning (Steinberg *et al*, 2013; Tsai *et al*, 2009; Witten *et al*, 2011), but can also result in addiction-like phenotypes in animals (Pascoli *et al*, 2015). It has been proposed that drugs of abuse and cues that predict these drugs, by increasing dopaminergic activity, will be processed as salient stimuli, thus promoting motivated behavior to obtain more drug (Robinson and Berridge, 2003). Although this is true for the initial drug experience, many have argued that over the course of addiction, neural control of drug-taking behaviors shifts to become dependent on non-dopaminergic mechanisms (Kalivas and Volkow, 2005). In support of this, human and animal studies have shown that extensive drug experience decreases the dopaminergic signaling in response to both drug and drug-associated cues over time despite increased salience and behavioral responses (ie, drug seeking/taking) to those cues (Volkow *et al*, 2014; Willuhn *et al*, 2014). By elucidating the brain-wide activity pattern evoked by TH<sup>VTA</sup> stimulation paired with a sensory stimulus, we show that dopamine-driven plasticity in this experiment is not limited to sensory cortices, but instead recruits numerous extrasensory brain regions, even in the absence of further dopaminergic signaling (ie, as seen during the postpairing paw stimulation). Taken together, our findings reveal a putative mechanism whereby drugs and drug-associated cues become

pathologically salient, particularly through dopamine-mediated recruitment of non-dopaminergic mechanisms during early drug use, such that these cues remain salient despite subsequent hypoactivity in the dopamine system as seen during later phases of addiction.

## FUNDING AND DISCLOSURE

The authors declare no conflict of interest.

## ACKNOWLEDGMENTS

We thank members of Stuber and Shih laboratories for discussion. We also thank the UNC vector core for viral packaging, and the UNC Neuroscience Center Microscopy Core (P30 NS045892). This study was supported by the Brain and Behavior Research Foundation, the Foundation of Hope, the Klarman Family Foundation, and the National Institute on Drug Abuse (DA032750, DA038168) (to GDS), and UNC Neurology-BRIC startup funds, University Research Council, and SeeCure LLC (to YYIS). HKD was supported by the National Institute on Drug Abuse (T32 Training Grant "Predoctoral Training in Addiction Science", DA041104), NS007431, and UNC Graduate Training Program in Translational Medicine supported by HHMI. VMKN was supported by the UNC Neuroscience Center's Helen Lyng White Fellowship in Neuroscience Research. JHJ was supported by MH104013. MD was supported by a Human Frontier Science Program Cross-Disciplinary Fellowship.

## AUTHOR CONTRIBUTIONS

HKD, YYIS and GDS designed the experiments. HKD, JHJ, JAM, PAK, YCJK, and MD collected data. KD and IBW provided critical reagents. VMKN, HKD, WG, SL, YYIS, and GDS analyzed data. GDS, HKD, and VMKN wrote the manuscript with input from all authors.

## REFERENCES

Andersen AH, Gash DM, Avison MJ (1999). Principal component analysis of the dynamic response measured by fMRI: a generalized linear systems framework. *Magn Reson Imaging* **17**: 795–815.

Aravanis AM, Wang L-P, Zhang F, Meltzer LA, Mogri MZ, Schneider MB et al (2007). An optical neural interface: *in vivo* control of rodent motor cortex with integrated fiberoptic and optogenetic technology. *J Neural Eng* **4**: S143–S156.

Bao S, Chan VT, Merzenich MM (2001). Cortical remodelling induced by activity of ventral tegmental dopamine neurons. *Nature* **412**: 79–83.

Berridge KC, Robinson TE (1998). What is the role of dopamine in reward: hedonic impact, reward learning, or incentive salience? *Brain Res Rev* **28**: 309–369.

Childress AR, Mozley PD, McElgin W, Fitzgerald J, Reivich M, O'Brien CP (1999). Limbic activation during cue-induced cocaine craving. *Am J Psychiatry* **156**: 11–18.

Chuhma N, Zhang H, Masson J, Zhuang X, Sulzer D, Hen R et al (2004). Dopamine neurons mediate a fast excitatory signal via their glutamatergic synapses. *Off J Soc Neurosci* **24**: 972–981.

Cohen JY, Haesler S, Vong L, Lowell BB, Uchida N (2012). Neuron-type-specific signals for reward and punishment in the ventral tegmental area. *Nature* **482**: 85–88.

Cox RW (1996). AFNI: software for analysis and visualization of functional magnetic resonance neuroimages. *Comput Biomed Res Int J* **29**: 162–173.

Day JJ, Roitman MF, Wightman RM, Carelli RM (2007). Associative learning mediates dynamic shifts in dopamine signaling in the nucleus accumbens. *Nat Neurosci* **10**: 1020–1028.

Desai M, Kahn I, Knoblich U, Bernstein J, Atallah H, Yang A et al (2011). Mapping brain networks in awake mice using combined optical neural control and fMRI. *J Neurophysiol* **105**: 1393–1405.

Di Chiara G, Imperato A (1988). Drugs abused by humans preferentially increase synaptic dopamine concentrations in the mesolimbic system of freely moving rats. *Proc Natl Acad Sci USA* **85**: 5274–5278.

Domingos AI, Vaynshteyn J, Voss HU, Ren X, Gradinaru V, Zang F et al (2011). Leptin regulates the reward value of nutrient. *Nat Neurosci* **14**: 1562–1568.

Eklund A, Nichols TE, Knutsson H (2016). Cluster failure: Why fMRI inferences for spatial extent have inflated false-positive rates. *Proc Natl Acad Sci USA* **113**: 7900–7905.

Ferenczi EA, Zalocusky KA, Liston C, Grosenick L, Warden MR, Amatya D et al (2016). Prefrontal cortical regulation of brainwide circuit dynamics and reward-related behavior. *Science* **351**: aac9698.

Freeman J, Vladimirov N, Kawashima T, Mu Y, Sofroniew NJ, Bennett DV et al (2014). Mapping brain activity at scale with cluster computing. *Nat Methods* **11**: 941–950.

Fukuda M, Vazquez AL, Zong X, Kim S-G (2013). Effects of the  $\alpha_2$ -adrenergic receptor agonist dexmedetomidine on neural, vascular and BOLD fMRI responses in the somatosensory cortex. *Eur. J. Neurosci.* **37**: 80–95.

Gee S, Ellwood I, Patel T, Luongo F, Deisseroth K, Sohal VS (2012). Synaptic activity unmasks dopamine D2 receptor modulation of a specific class of layer V pyramidal neurons in prefrontal cortex. *J Neurosci* **32**: 4959–4971.

Gerits A, Farivar R, Rosen BR, Wald LL, Boyden ES, Vanduffel W (2012). Optogenetically induced behavioral and functional network changes in primates. *Curr Biol* **22**: 1722–1726.

Hnasko TS, Chuhma N, Zhang H, Goh GY, Sulzer D, Palmiter RD et al (2010). Vesicular glutamate transport promotes dopamine storage and glutamate corelease *in vivo*. *Neuron* **65**: 643–656.

Jacob SN, Ott T, Nieder A (2013). Dopamine regulates two classes of primate prefrontal neurons that represent sensory signals. *Off J Soc Neurosci* **33**: 13724–13734.

Jennings JH, Sparta DR, Stamatakis AM, Ung RL, Pleil KE, Kash TL et al (2013). Distinct extended amygdala circuits for divergent motivational states. *Nature* **496**: 224–228.

Kahn I, Desai M, Knoblich U, Bernstein J, Henninger M, Graybiel AM et al (2011). Characterization of the functional MRI response temporal linearity via optical control of neocortical pyramidal neurons. *Off J Soc. Neurosci.* **31**: 15086–15091.

Kalivas PW, Volkow ND (2005). The neural basis of addiction: a pathology of motivation and choice. *Am. J. Psychiatry* **162**: 1403–1413.

Kapur S (2003). Psychosis as a state of aberrant salience: a framework linking biology, phenomenology, and pharmacology in schizophrenia. *Am J Psychiatry* **160**: 13–23.

Kim S-G, Harel N, Jin T, Kim T, Lee P, Zhao F (2013). Cerebral blood volume MRI with intravascular superparamagnetic iron oxide nanoparticles. *NMR Biomed* **26**: 949–962.

Koob GF, Volkow ND (2009). Neurocircuitry of addiction. *Neuropsychopharmacology* **35**: 217–238.

Lai H-Y, Albaugh DL, Kao Y.-C.J., Younce JR, Shih Y.-Y.I. (2015). Robust deep brain stimulation functional MRI procedures in rats and mice using an MR-compatible tungsten microwire electrode. *Magn Reson Med* **73**: 1246–1251.

Lammel S, Steinberg EE, Földy C, Wall NR, Beier K, Luo L et al (2015). Diversity of transgenic mouse models for selective targeting of midbrain dopamine neurons. *Neuron* **85**: 429–438.

- Lavin A, Nogueira L, Lapish CC, Wightman RM, Phillips PEM, Seamans JK (2005). Mesocortical dopamine neurons operate in distinct temporal domains using multimodal signaling. *Off J Soc Neurosci* **25**: 5013–5023.
- Lee JH, Durand R, Gradinaru V, Zhang F, Goshen I, Kim D-S et al (2010). Global and local fMRI signals driven by neurons defined optogenetically by type and wiring. *Nature* **465**: 788–792.
- Lein ES, Hawrylycz MJ, Ao N, Ayres M, Bensinger A, Bernard A et al (2007). Genome-wide atlas of gene expression in the adult mouse brain. *Nature* **445**: 168–176.
- Leite FP, Tsao D, Vanduffel W, Fize D, Sasaki Y, Wald LL et al (2002). Repeated fMRI using iron oxide contrast agent in awake, behaving macaques at 3 Tesla. *NeuroImage* **16**: 283–294.
- Lewis BL, O'Donnell P (2000). Ventral tegmental area afferents to the prefrontal cortex maintain membrane potential 'up' states in pyramidal neurons via D1 dopamine receptors. *Cereb Cortex* **10**: 1168–1175.
- Mandeville JB, Marota JJ, Kosofsky BE, Keltner JR, Weissleder R, Rosen BR et al (1998). Dynamic functional imaging of relative cerebral blood volume during rat forepaw stimulation. *Magn. Reson. Med. Soc.* **39**: 615–624.
- Marder E (2012). Neuromodulation of neuronal circuits: back to the future. *Neuron* **76**: 1–11.
- Marota JJ, Mandeville JB, Weisskoff RM, Moskowitz MA, Rosen BR, Kosofsky BE (2000). Cocaine activation discriminates dopaminergic projections by temporal response: an fMRI study in Rat. *NeuroImage* **11**: 13–23.
- Monti MM (2011). Statistical analysis of fMRI time-series: a critical review of the GLM approach. *Front Hum Neurosci* **5**: 28.
- Otani S, Daniel H, Roisin M-P, Crepel F (2003). Dopaminergic modulation of long-term synaptic plasticity in rat prefrontal neurons. *Cereb Cortex* **13**: 1251–1256.
- Pascoli V, Terrier J, Hiver A, Lüscher C (2015). Sufficiency of mesolimbic dopamine neuron stimulation for the progression to addiction. *Neuron* **88**: 1054–1066.
- Paxinos G, Watson C. *The Rat Brain In Stereotaxic Coordinates*, 5th edn. Elsevier Academic Press: Burlington, 2005.
- Phillips PEM, Stuber GD, Heien M.L.A.V., Wightman RM, Carelli RM (2003). Subsecond dopamine release promotes cocaine seeking. *Nature* **422**: 614–618.
- Robinson TE, Berridge KC (2003). Addiction. *Annu Rev Psychol* **54**: 25–53.
- Roitman MF, Stuber GD, Phillips PEM, Wightman RM, Carelli RM (2004). Dopamine operates as a subsecond modulator of food seeking. *Off J Soc. Neurosci.* **24**: 1265–1271.
- Roitman MF, Wheeler RA, Wightman RM, Carelli RM (2008). Real-time chemical responses in the nucleus accumbens differentiate rewarding and aversive stimuli. *Nat. Neurosci.* **11**: 1376–1377.
- Salamone JD, Correa M, Farrar A, Mingote SM (2007). Effort-related functions of nucleus accumbens dopamine and associated forebrain circuits. *Psychopharmacology (Berl.)* **191**: 461–482.
- Schultz W (1998). Predictive reward signal of dopamine neurons. *J Neurophysiol* **80**: 1–27.
- Shih Y.-Y.I., Chen C.-C.V., Shyu B-C, Lin Z-J, Chiang Y-C, Jaw F-S et al (2009). A new scenario for negative functional magnetic resonance imaging signals: endogenous neurotransmission. *J Neurosci* **29**: 3036–3044.
- Shih Y.-Y.I., Wang L, De La Garza BH, Li G, Cull G, Kiel JW et al (2013). Quantitative retinal and choroidal blood flow during light, dark adaptation and flicker light stimulation in rats using fluorescent microspheres. *Curr Eye Res* **38**: 292–298.
- Shih Y.-Y.I., Huang S, Chen Y-Y, Lai H-Y, Kao Y.-C.J., Du F et al (2014a). Imaging neurovascular function and functional recovery after stroke in the rat striatum using forepaw stimulation. *J Cereb Blood Flow Metab* **34**: 1483–1492.
- Shih Y.-Y.I., Yash TV, Rogers B, Duong TQ (2014b). FMRI of deep brain stimulation at the rat ventral posteromedial thalamus. *Brain Stimulat* **7**: 190–193.
- Smirnakis SM, Schmid MC, Weber B, Tolia AS, Augath M, Logothetis NK (2007). Spatial specificity of BOLD versus cerebral blood volume fMRI for mapping cortical organization. *J Cereb Blood Flow Metab* **27**: 1248–1261.
- Solt K, Van Dort CJ, Chemali JJ, Taylor NE, Kenny JD, Brown EN (2014). Electrical stimulation of the ventral tegmental area induces reanimation from general anesthesia. *Anesthesiology* **121**: 311–319.
- Sparta DR, Stamatakis AM, Phillips JL, Hovelsø N, van Zessen R, Stuber GD (2012). Construction of implantable optical fibers for long-term optogenetic manipulation of neural circuits. *Nat Protoc* **7**: 12–23.
- Steinberg EE, Keiflin R, Boivin JR, Witten IB, Deisseroth K, Janak PH (2013). A causal link between prediction errors, dopamine neurons and learning. *Nat Neurosci* **16**: 966–973.
- Stuber GD, Roitman MF, Phillips PEM, Carelli RM, Wightman RM (2005a). Rapid dopamine signaling in the nucleus accumbens during contingent and noncontingent cocaine administration. *Off Publ Am Coll Neuropsychopharmacol* **30**: 853–863.
- Stuber GD, Wightman RM, Carelli RM (2005b). Extinction of cocaine self-administration reveals functionally and temporally distinct dopaminergic signals in the nucleus accumbens. *Neuron* **46**: 661–669.
- Stuber GD, Klanker M, de Ridder B, Bowers MS, Joosten RN, Feenstra MG et al (2008). Reward-predictive cues enhance excitatory synaptic strength onto midbrain dopamine neurons. *Science* **321**: 1690–1692.
- Stuber GD, Hnasko TS, Britt JP, Edwards RH, Bonci A (2010). Dopaminergic terminals in the nucleus accumbens but not the dorsal striatum corelease glutamate. *Off J Soc Neurosci* **30**: 8229–8233.
- Stuber GD, Sparta DR, Stamatakis AM, van Leeuwen WA, Hardjoprajitno JE, Cho S et al (2011). Excitatory transmission from the amygdala to nucleus accumbens facilitates reward seeking. *Nature* **475**: 377–380.
- Surmeier DJ, Ding J, Day M, Wang Z, Shen W (2007). D1 and D2 dopamine-receptor modulation of striatal glutamatergic signaling in striatal medium spiny neurons. *Trends Neurosci.* **30**: 228–235.
- Swanson LW (1982). The projections of the ventral tegmental area and adjacent regions: a combined fluorescent retrograde tracer and immunofluorescence study in the rat. *Brain Res Bull* **9**: 321–353.
- Tritsch NX, Ding JB, Sabatini BL (2012). Dopaminergic neurons inhibit striatal output through non-canonical release of GABA. *Nature* **490**: 262–266.
- Tritsch NX, Oh W-J, Gu C, Sabatini BL (2014). Midbrain dopamine neurons sustain inhibitory transmission using plasma membrane uptake of GABA, not synthesis. *eLife* **3**: e01936.
- Tsai H-C, Zhang F, Adamantidis A, Stuber GD, Bonci A, de Lecea L et al (2009). Phasic firing in dopaminergic neurons is sufficient for behavioral conditioning. *Science* **324**: 1080–1084.
- Tye KM, Mirzabekov JJ, Warden MR, Ferenczi EA, Tsai H-C, Finkelstein J et al (2013). Dopamine neurons modulate neural encoding and expression of depression-related behaviour. *Nature* **493**: 537–541.
- Volkow ND, Fowler JS, Wang G-J, Swanson JM (2004). Dopamine in drug abuse and addiction: results from imaging studies and treatment implications. *Mol. Psychiatry* **9**: 557–569.
- Volkow ND, Tomasi D, Wang G-J, Logan J, Alexoff DL, Jayne M et al (2014). Stimulant-induced dopamine increases are markedly blunted in active cocaine abusers. *Mol. Psychiatry* **19**: 1037–1043.
- Willuhn I, Burgeno LM, Groblewski PA, Phillips PEM (2014). Excessive cocaine use results from decreased phasic dopamine signaling in the striatum. *Nat Neurosci* **17**: 704–709.
- Witten IB, Steinberg EE, Lee SY, Davidson TJ, Zalocusky KA, Brodsky M et al (2011). Recombinase-driver rat lines: tools,

- techniques, and optogenetic application to dopamine-mediated reinforcement. *Neuron* **72**: 721–733.
- Worsley KJ, Friston KJ (1995). Analysis of fMRI time-series revisited—again. *NeuroImage* **2**: 173–181.
- Worsley KJ, Liao CH, Aston J, Petre V, Duncan GH, Morales F *et al* (2002). A general statistical analysis for fMRI data. *NeuroImage* **15**: 1–15.
- Yamamoto H, Fujimori T, Sato H, Ishikawa G, Kami K, Ohashi Y (2014). Statistical hypothesis testing of factor loading in principal component analysis and its application to metabolite set enrichment analysis. *BMC Bioinform* **15**: 51.
- Younce JR, Albaugh DL, Shih Y-YI (2014). Deep brain stimulation with simultaneous FMRI in rodents. *J Vis Exp* **84**: 1–7.

Supplementary Information accompanies the paper on the Neuropsychopharmacology website (<http://www.nature.com/npp>)